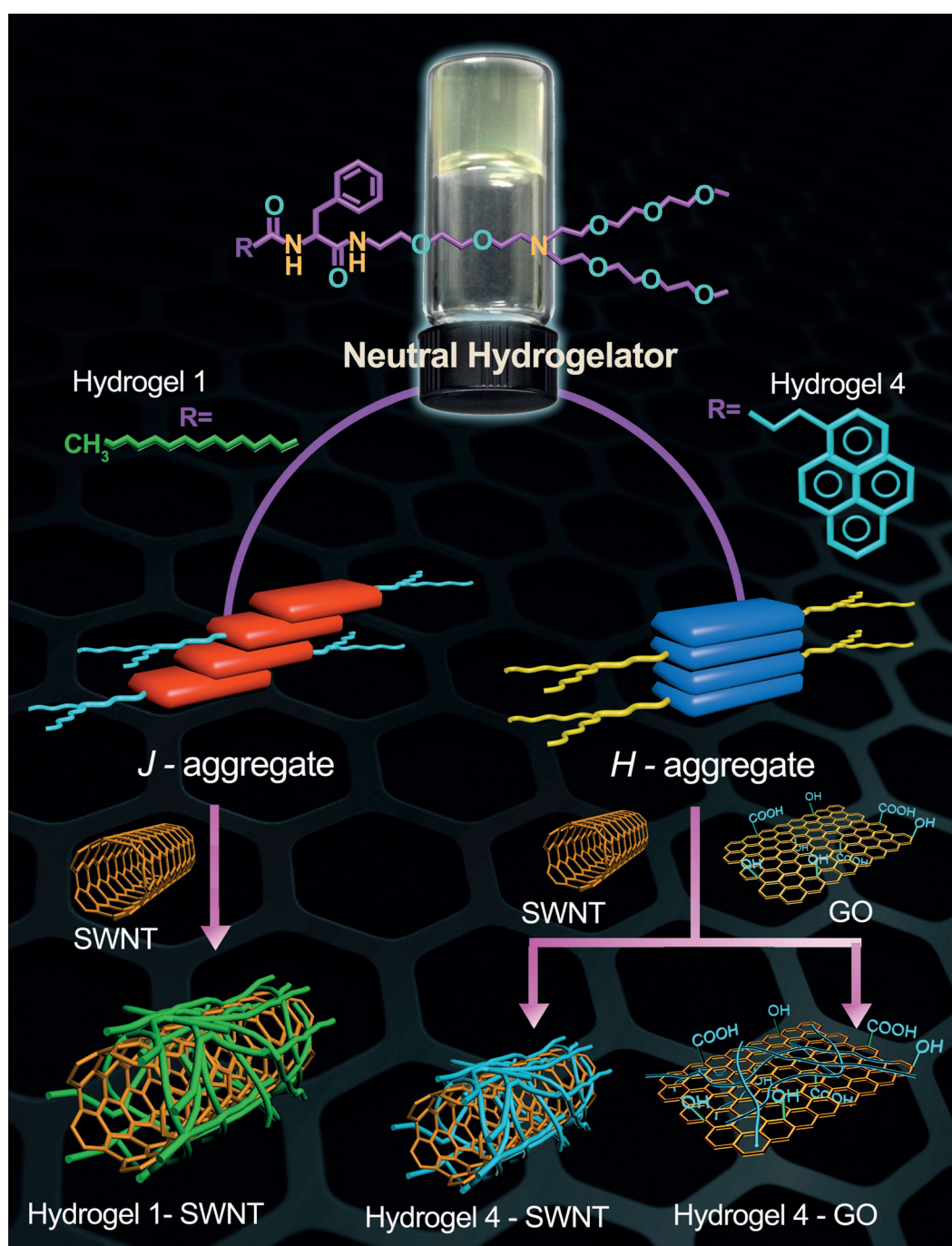


Neutral Hydrogels | *Hot Paper* |

Hydrophobic End-Modulated Amino-Acid-Based Neutral Hydrogelators: Structure-Specific Inclusion of Carbon Nanomaterials

Pritam Choudhury, Deep Mandal, Sayanti Brahmachari, and Prasanta Kumar Das^{*[a]}



Abstract: Hydrophobic end-modulated L-phenylalanine-containing triethylene glycol monomethyl ether tagged neutral hydrogelators (**1–4**) are developed. Investigations determine the gelators' structure-dependent inclusion of carbon nanomaterials (CNMs) in the self-assembled fibrillar network (SAFIN). The gelators (**1**, **3**, and **4**) can immobilize water and aqueous buffer (pH 3–7) with a minimum gelator concentration of 10–15 mg mL⁻¹. The hydrophobic parts of the gelators are varied from a long chain (C-16) to an extended aromatic pyrenyl moiety, and their abilities to integrate 1D and 2D allotropes of carbon (i.e., single-walled carbon nanotubes (SWNTs) and graphene oxide (GO), respectively) within the gel are investigated. Gelator **1**, containing a long alkyl

chain (C-16), can include SWNTs, whereas the pyrene-containing **4** can include both SWNTs and GO. Gelator **3** fails to incorporate SWNTs or GO owing to its slow rate of gelation and possibly a mismatch between the aggregated structure and CNMs. The involvement of various forces in self-aggregated gelation and physicochemical changes occurring through CNM inclusion are examined by spectroscopic and microscopic techniques. The distinctive pattern of self-assembly of gelators **1** and **4** through *J*- and *H*-type aggregation might facilitate the structure-specific CNM inclusion. Inclusion of SWNTs/GO within the hydrogel matrix results in a reinforcement in mechanical stiffness of the composites compared with that of the native hydrogels.

Introduction

The development of self-assembled materials has been an expanding research area in the last few decades because of their versatile physicochemical properties as well as their mounting applications in diverse areas including drug delivery, sensors, template materials, and so forth.^[1–6] Low-molecular-weight gelators (LMWGs) are small organic molecules that have an ability to restrict the mobility of solvents through the formation of a self-assembled fibrillar network (SAFIN). Gelation of small molecules is an outcome of a balanced combination of various interactions such as hydrogen bonding, π – π stacking, van der Waals forces, and so on.^[7] An optimal balance between hydrophobicity and hydrophilicity of the amphiphile play the key role in the formation of SAFINs.^[6] In recent years, the development of neutral hydrogels at physiological salinity has gained importance owing to its suitability for bio-medicinal applications.^[8] The design of a neutral hydrogelator, devoid of any charged moiety, and which can form a gel in pure water or buffer solutions at neutral pH, is a very tricky task. In this context, the presence of a strong hydrophilic moiety (without any charged residue) in the gelator's structure would be the key factor toward the rational design of a neutral hydrogelator. In addition, a hydrophobic moiety and a residue capable of participating in intermolecular hydrogen bonding need to be included within the gelator's structure to maintain the required hydrophilic–lipophilic balance (HLB) for self-assembled gelation.

Simultaneously with rapid structural advancement, researchers are trying to build up soft nanocomposites composed of

nanomaterial-integrated gel, with the objective of improving its physicochemical properties. Hybrid gels (containing nanomaterials) with improved mechanical stiffness are finding applications in the area of supercapacitors, nanoelectronics, photovoltaic devices, chemical sensors, biomedicine, and so on.^[7a,8,9] Exogenous nanomaterials such as carbon nanotubes (CNTs), graphene, graphene oxide (GO), silver nanoparticles, gold nanoparticles, and so on, have been included in the interstitial spaces of SAFINs, and aided advantageous changes in their properties.^[10,11] However, it is difficult to predict the inclusion of carbon nanomaterials (CNMs) within the fibrillar network; there may be a dependence on the physical dimensions of the CNMs as well as on the structure of the amphiphilic gelator. Reports on the structure dependence of specific integration in the gelator of different CNMs within SAFINs are scarce. Distinctive structural and self-aggregation properties of the gelator would play a vital role in the integration of CNMs within a hydrogel. Hence, it would be highly intriguing to design neutral hydrogelators, as well as to find a correlation between molecular-structure-dependent aggregation and selective inclusion of CNMs within the hydrogel matrix.

Herein, we report the rational design of neutral hydrogelators composed of hydrophobic terminal-group-modulated L-phenylalanine with triethylene glycol monomethyl ether (TEG)-tagged hydrophilic moiety (**1–4**, Figure 1). Amphiphiles **1**, **3**, and **4** were found to form self-assembled hydrogels in water and aqueous buffer solutions of varying pH values ranging from 3.0–7.0. Amphiphile **2** self-aggregated to form a gel in a DMSO/water mixture (1:3, v/v). The hydrophobic end of the gelator molecule was judiciously varied from a long alkyl chain (C-16) to an extended aromatic pyrenyl moiety to monitor the selective CNM inclusion behavior of the hydrogels. The long chain (C-16)-containing gelator **1** efficiently disperses and includes 1D allotropes of carbon, single-walled carbon nanotubes (SWNTs) within the gel matrix. Notably, the pyrene-containing gelator **4** was able to integrate both 1D and 2D allotropes of carbon (i.e., SWNTs and GO) in its SAFIN. The self-aggregation behavior of the amphiphilic molecules and inclusion of different carbon nanomaterials within the SAFINs were studied by spectroscopic and microscopic means. The mechanical

[a] P. Choudhury, D. Mandal, S. Brahmachari, Prof. P. K. Das
Department of Biological Chemistry
Indian Association for the Cultivation of Science
Jadavpur, Kolkata, 700032 (India)
E-mail: bcpcd@iacs.res.in

Supporting information for this article can be found under <http://dx.doi.org/10.1002/chem.201504888>. This includes the synthetic schemes of **1–4**, characterization of gelators **1–4** (¹H NMR, mass spectrometry, CHN data), UV/Vis absorbance spectra and XRD spectra of GO, TEM image of the dried hydrogel **1**, CD spectra of **1** and **4** in absence and presence of SWNT/GO, FTIR spectra of xerogels of **1**, **4**, 1-SWNT, 4-SWNT, and 4-GO.

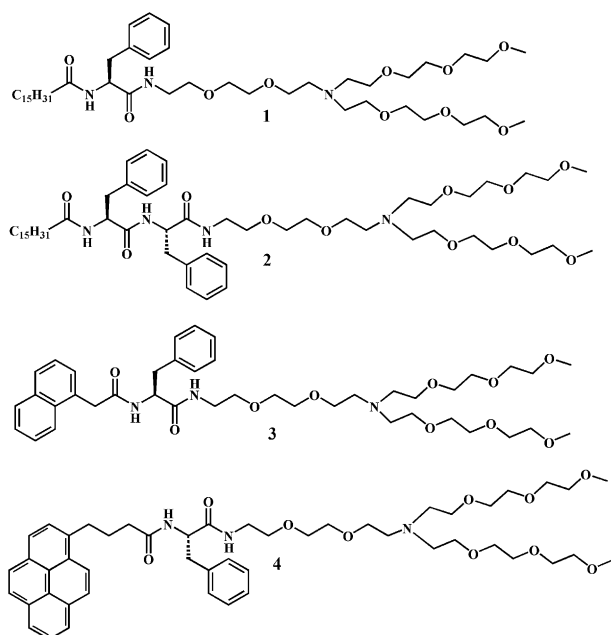


Figure 1. Structures of the amphiphilic gelators 1–4.

stiffness of the gel and CNM–gel composite was monitored by rheological measurements.

Results and Discussion

The development of a neutral amphiphilic molecule with hydrogelation ability is of high importance. Moreover, such a gelator's structure-dependent inclusion of CNMs within the hydrogel is a very interesting research domain, which has not been well explored. In this present study, we developed neutral gelators that form hydrogels in water and aqueous buffer, and tried to understand the influence of the gelator structure on specific CNM integration in its SAFIN. Accordingly, the hydrogelators (1–4, Figure 1, Schemes S1 and S2, Supporting Information) were synthesized by coupling between the C-terminus of L-phenylalanine and the twin-chain hydrophilic triethylene glycol monomethyl ether (TEG) moiety attached to 2,2'-(ethylenedioxy)bis(ethylamine). The N-terminus of the L-phenylalanine was coupled through an amide linkage by different hydrophobic groups such as C-16 (1), an additional L-phenylalanine linked with C-16 (2), naphthalene (3), and pyrene (4). The hydrophobicity of the gelator was judiciously varied from a long alkyl chain to an extended aromatic group to study their aggregation pattern as well as their influence on CNM inclusion. With the aim of developing a neutral gelator, it is essential to choose a specific hydrophilic moiety that is devoid of any charged unit as well as being able to maintain the optimal HLB required for hydrogelation. Hence, we chose the TEG moiety as the hydrophilic terminus. The hydrophilic TEG-substituted 2,2'-(ethylenedioxy)bis(ethylamine) group enhanced the solubility of the gelator in aqueous solvents, and the hydrophobicity of C-16 to pyrene might have maintained the necessary HLB for self-assembled gelation. The linker amino acid

also contributed to the gelation through possible intermolecular hydrogen bonding.^[5,10a,b,j]

We investigated the hydrogelation efficiency of the neutral amphiphiles 1–4 in water, aqueous phosphate buffer of pH 3–7, and DMSO–water mixture (1:3, v/v) (Table 1). Initially, amphiphile 1, containing the C-16 alkyl chain, formed a gel in water with a minimum gelation concentration (MGC) of 15 mg mL⁻¹.

Table 1. Minimum gelation concentrations (MGCs) of 1–4 in different aqueous media.

Solvents	1 [mg mL ⁻¹]	2 [mg mL ⁻¹]	3 [mg mL ⁻¹]	4 [mg mL ⁻¹]
Milli-Q water	15.0	Ins ^[b]	14.0	10.0
pH 7	15.3	Ins	11	11.0
pH 6	15.1	Ins	11	9.4
pH 5	Sol ^[a]	Ins	Sol	8.8
pH 3	Sol	12.0	Sol	Sol
DMSO–water (1:3, v/v)	Sol	10.0	Sol	10.5

[a] Sol = Soluble, [b] Ins = Insoluble.

The formation of the gel was confirmed from the “stable-to-inversion” state of the glass vial (diameter 10 mm). With the expectation of improving the MGC, we incorporated an additional L-phenylalanine in amphiphile 2, which might aid gelation through its extra amide bond and additional aromatic residue. To our surprise, 2 did not form a gel in water. However, it showed efficient gelation in the DMSO–water mixture (1:3, v/v) at MGC = 10 mg mL⁻¹. Presumably, amphiphile 2 has lost the critical HLB required for self-aggregation in water owing to the presence of an extra phenyl ring compared with 1. Subsequently, instead of the C-16 alkyl chain, we switched to an aromatic hydrophobic unit, that is, naphthalene-containing amphiphile 3, keeping all other structural components the same as in 1. Amphiphile 3 showed hydrogelation ability in water at MGC = 14 mg mL⁻¹, but at a very slow rate. It took almost five days to form a gel that was stable to inversion in the glass vial. Generally, it was found that the presence of an extended aromatic ring in the amphiphile's structure facilitates self-assembled gelation. Hence, we introduced a pyrenyl moiety instead of naphthalene in amphiphile 4 with the aim of improving the gelation efficiency. Amphiphile 4 was found to gelate in water with improved efficiency (MGC = 10 mg mL⁻¹). The decrease in MGC compared with 1 and 3, (which gelate in pure water) is probably caused by the additional π – π stacking interaction between pyrenyl moieties.^[7a,10b] We also monitored the gelation abilities of 1–4 in phosphate–HCl buffer of pH 3.0–7.0 (Table 1). It was found that amphiphiles 1, 3, and 4 can form hydrogels at pH 6.0 and 7.0, whereas amphiphile 2 shows gelation ability only at pH 3.0. Additionally, amphiphile 4 can also form a hydrogel at pH 5.0. Presumably, the tertiary nitrogen present at the terminus of the gelator motif gives rise to the pH-responsive hydrogelation behavior through protonation at different pH values.^[10b] All the amphiphiles remain soluble in DMSO, and amphiphiles 2 and 4 can immobilize DMSO–water solvent mixture (1:3, v/v) to form gels at MGC values of 10 and

10.5 mg mL⁻¹, respectively. Among the four amphiphiles, **4** showed a better gelation efficiency in pure water and in aqueous buffer solutions, possibly owing to the presence of the extended aromatic ring (pyrenyl moiety), which may facilitate additional π - π interactions. Thus, with variation in the hydrophobic unit of the gelator's structure, the gelation efficiency also modulated, presumably owing to the alteration in the overall HLB of the amphiphile.

On the basis of the observed gelation, we chose hydrogelators **1**, **3**, and **4** for inclusion of various CNMs within the hydrogel matrix. Gelator **2** was not considered for this study because of its inefficiency in forming a hydrogel in pure water as well as in pH 7.0 phosphate-HCl buffer solution. We selected two types of CNMs for integration within the hydrogel: a 1D allotrope of carbon [single-walled pristine carbon nanotubes (SWNTs)] and a 2D allotrope of carbon [graphene oxide (GO)].^[11] For effective inclusion of these CNMs in the gel matrix, they should be well dispersed in the aqueous medium in the presence of the amphiphile. Accordingly, we first tried to disperse the amphiphobic pristine SWNTs using amphiphiles **1**, **3**, and **4**.^[10b] Briefly, SWNTs (1 mg) were put in amphiphile solution (4 mL, 2.5 mg mL⁻¹) and subjected to tip sonication followed by bath sonication. The suspension was then centrifuged at 6000 rpm for 30 min. The supernatant was collected, and the amount of dispersed SWNTs was calculated using the calibration plot prepared with sodium dodecylbenzenesulfonate (SDBS).^[8c] Amphiphiles **1** and **4** showed SWNT dispersion abilities of 190 and 210 $\mu\text{g mL}^{-1}$, respectively. On the other hand, amphiphile **3** showed moderate SWNT dispersion (55 $\mu\text{g mL}^{-1}$), probably owing to its slow rate of self-assembly. Upon confirmation of the SWNT dispersion abilities of **1**, **3**, and **4**, amphiphiles were taken at the respective MGCs (15 mg mL⁻¹ for **1** and **3**, and 10 mg mL⁻¹ for **4**) in water and sonicated after mixing with required amount of SWNTs. The mixtures were then left to stand for 30 min. The formation of the SWNT-gel composite was tested through the "stable-to-inversion" test of the glass vial (Figure 2). SWNTs were successfully included in the hydrogel matrices of **1** and **4**, giving **1**-SWNT and **4**-SWNT nanohybrids, respectively, whereas **3** showed poor SWNT inclusion owing to its slow rate of gelation (Figure 2). In the absence of any amphiphiles, SWNTs remain insoluble in water.

We monitored the maximum inclusion amount of SWNTs within hydrogels **1** and **4** by varying the SWNT concentration (0.25–6.0 mg mL⁻¹, Table 2) without compromising the stability of the gel. Hydrogels **1** and **4** maximally accommodate 3.0 and 5.0 mg mL⁻¹ SWNTs, respectively, at their MGCs. The successful inclusion of SWNTs in the entangled gel network may be attributed to the comparable morphology and dimensions of

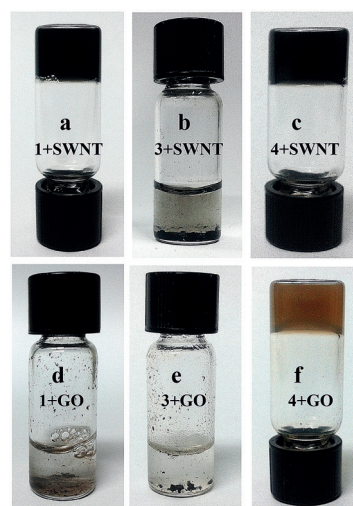


Figure 2. Inclusion and precipitation of SWNTs and GO in hydrogels of **1**, **3**, and **4**.

SWNTs with the gel fibers. The efficient dispersion of SWNTs in aqueous solutions of amphiphiles **1** and **4** might have facilitated the successful inclusion of SWNTs within the gel matrix. At this instant, we attempted to include the 2D allotrope of carbon, GO, within the SAFIN of the hydrogel. Accordingly, GO was synthesized from graphite powder through a modified Hummer's method and characterized as described in the Experimental Section (Figure S1, Supporting Information).^[12a] The freshly prepared GO and gelators (**1**, **3**, and **4**) at their MGCs were put in milli-Q water and probe-sonicated for 10 min at 40% power output. The resulting mixtures were then allowed to cool at room temperature. Intriguingly, in the presence of GO, gelator **1** lost its hydrogelation ability, and GO precipitated out from the solution (Figure 2). Similarly, amphiphile **3** was also unable to include GO in its matrix (Figure 2). Interestingly, only hydrogel **4** at its MGC (10 mg mL⁻¹ in water) formed the GO-included hydrogel **4** (4-GO) nanocomposite. The highest inclusion ability of GO within hydrogel **4** was noted to be 5 mg mL⁻¹ (Figure 2). It is probable that the pyrenyl moiety present in gelator **4** aided the inclusion of GO through hydrophobic and π - π interactions to form the 4-GO composite.

It is apparent from the above observations that CNM inclusion ability within the hydrogel matrix is not the same for all the gelators. Gelator **1** containing the C-16 long chain was able to include the 1D allotrope of carbon (SWNTs) in its SAFIN, but failed to integrate the 2D allotrope (GO). Gelator **3** was unable to integrate either SWNTs or GO. Presumably, the naphthalene unit in gelator **3** does not provide the required hydrophobicity to facilitate its interaction with the aromatic backbone of SWNTs and GO. Also, there could be a mismatch between the aggregated structure of **3** and the CNMs. Gelator **4** showed an ability to include both the 1D (SWNTs) and 2D (GO) allotropes of carbon. The successful integration of SWNTs and GO within the hydrogel **4** matrix might be attributed to the additional π - π interaction of gelator **4** originating from the pyrenyl group. The ultrathin honeycomb-like planar structure of GO and the aromatic backbone of SWNTs may fit between the extended ar-

Table 2. Maximum accommodation of pristine SWNTs and GO in hydrogels of **1** and **4** at their MGCs at 25 °C.

Gelator	[SWNT] in hydrogel [mg mL ⁻¹]	[GO] in hydrogel [mg mL ⁻¹]
1	3.0	–
4	5.0	5.0

omatic ring (pyrenyl moiety) through π - π stacking as well as van der Waals' interactions, leading to the successful formation of the 4-GO/SWNT nanocomposite.^[10f,12b] Thus, modulation of the hydrophobicity in the gelators' structures leads to structure-dependent inclusion of different CNMs in the gel matrices.

Microscopic studies

The supramolecular morphologies of the individual gels as well as SWNT/GO-integrated gels were investigated by transmission electron microscopy (TEM). The TEM images of native hydrogels **1**, **3**, and **4** in water and **2** in DMSO-water (1:3, v/v) medium showed entangled fibrillar networks with fibers of 20–50 nm in thickness (Figure 3 a–d). The helical nature of the gel fibers of hydrogel **1** was observed upon magnification of the TEM image (Figure S2, Supporting Information). Incorporation of SWNTs in hydrogel **1** led to a change in the morphology of the 1-SWNT composite (Figure 3 e). The extent of the criss-crossed intertwined network increased in the aggregated structure of the 1-SWNT composite compared with that of native gel **1**.^[10a] In the case of the 4-SWNT composite (Figure 3 f), a denser fibrillar network was observed, with thicker fibers (diameter 70–80 nm) than those of the native hydrogel **4**.^[10b] Upon inclusion of GO in hydrogel **4** (Figure 3 g), a very thin layered structure of GO sheet interlinked with gel fibers in a 3D network was noted.^[11b] The coexistence of the intertwined fibrillar network of gelator **4** and the entrapped GO sheet was also seen clearly from the scanning electron microscopy (SEM) image of the 4-GO composite (Figure 3 h). Interestingly, the diameter of the fibers was comparable in the native gel and the 4-GO nanohybrid, which indicates that inclusion of GO in the gel matrix did not perturb the self-assembly of **4**.^[11b] The microscopic images of the native gel and CNMs-gel composite revealed the gelator's successful, structure-dependent inclusion of different CNMs within the SAFIN of the hydrogel.

Determination of gel-to-sol transition temperature (T_{gel})

The native hydrogels and SWNT/GO-gel nanocomposites were thermoreversible in nature and also stable at room temperature for several months. The temperature at which the gel transforms to solution is known as the gel melting temperature or gel-to-sol transition temperature (T_{gel}).^[10b,j] For hydrogels **1**, **3**, and **4** (at their MGC in water), the T_{gel} values were found to be 57, 61, and 65 °C, respectively, and for hydrogel **2** (at MGC in DMSO-water, 1:3 v/v) T_{gel} was 56 °C. Interestingly, the T_{gel} values of the CNMs-included hydrogel (at MGCs) nanohybrids were found to be higher than those of the native gels. In the case of 1-SWNT ([SWNT]=3 mg mL⁻¹), 4-SWNT ([SWNT]=5 mg mL⁻¹), and 4-GO ([GO]=5 mg mL⁻¹), the measured T_{gel} values were 65, 73, and 75 °C, respectively. The increment in T_{gel} values of the SWNT/GO-gel nanocomposites might be caused by the enhancement in crosslinking fibers between SAFIN and CNMs in the gel matrix. Consequently, a higher energy/temperature was required to break the self-assembly of the CNM-gel composites.

Circular dichroism (CD) study

CD spectroscopy is known to provide information about the self-aggregation pattern of small-molecular-mass gelators.^[13] We have found different CD spectral patterns for the self-assembly of hydrogelators of **1**, **3**, and **4** (Figure 4). The CD spectrum of **1** (1 mg mL⁻¹ in milli-Q water) showed a negative cotton effect with double minima at 202 and 213 nm. The presence of double minima (202 and 213 nm) in the CD spectra indicates α -helicity in its self-aggregation (by its pattern but not by the position of the double minima).^[10b,13] The helical morphology of **1** is in concurrence with the corresponding TEM image of hydrogel **1** (Figure S2, Supporting Information). On the other hand, self-assembly of gelator **3** (1 mg mL⁻¹ in milli-Q water) showed a β -sheet pattern (positive band at

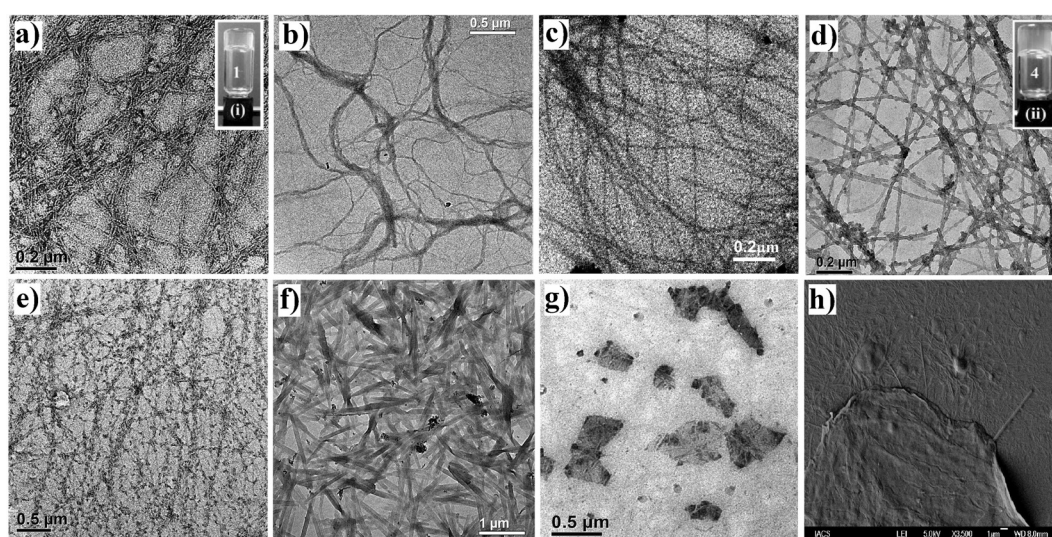


Figure 3. TEM images of hydrogels **1–4** (a–d, respectively). Insets of (a) and (d) show photographic images of hydrogels **1** and **4**, respectively. TEM images of e) 1-SWNT, f) 4-SWNT, and g) 4-GO composites. h) SEM image of 4-GO.

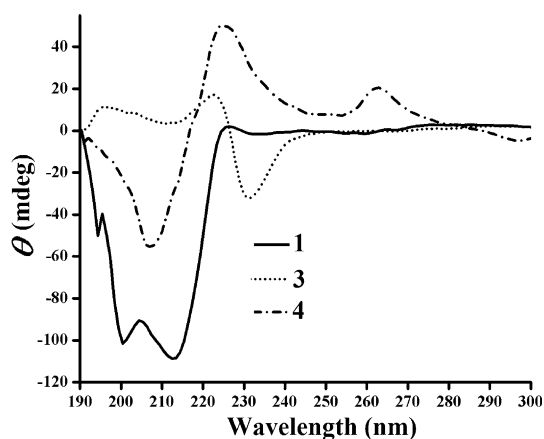


Figure 4. CD spectra of amphiphilic gelators 1, 3, and 4.

222 nm and negative band at 231 nm, Figure 4) in its CD spectra.^[13] In the case of gelator 4 (1 mg mL⁻¹ in milli-Q water), the CD spectra showed a positive band at 226 nm and negative band at 207 nm. This type of CD spectral pattern corroborates with β -turn-like self-aggregation.^[13d] Hence, the hydrophobic end modulation in the gelator's structure resulted in the formation of a distinctly different pattern of self-assembly for amphiphiles 1, 3, and 4. Presumably, these structure-dependent distinctive self-aggregation patterns of the hydrogelators helped to integrate different CNMs in the gel matrix in a selective manner. Moreover, the CD spectral patterns of 1 and 4 in the presence of SWNTs/GO (1-SWNT, 4-SWNT, and 4-GO composites) remain unaltered with a slight decrease in CD signal intensity (Figure S3, Supporting Information). This observation revealed the unperturbed arrangement of the supramolecular network formed by 1 and 4 upon inclusion of CNM in the hydrogel matrix.

FTIR spectroscopy

The influence of different kinds of noncovalent interactions during the gelation process was investigated from FTIR spectra of 1 and 4 recorded in the non-aggregated state (in chloroform) as well as in the gel state (in D₂O, Figure 5).^[10a,b] The FTIR spectrum of 1 in CHCl₃ showed transmittance peaks at approximately $\nu=3292$, 1643, and 1515 cm⁻¹, which originated from ν_{N-H} (amide A), amide $\nu_{C=O}$ (amide I), and ν_{N-H} (amide II) vibrations, respectively (Figure 5a). These peaks shifted to approximately $\nu=3377$ –3458 (broad band), 1617, and 1549 cm⁻¹ in D₂O. Analogous results were found for gelator 4, for which the transmittance peaks ν_{N-H} (amide A)=3300 cm⁻¹, amide $\nu_{C=O}$ (amide I)=1643 cm⁻¹, and ν_{N-H} (amide II)=1532 cm⁻¹ were shifted to ν_{N-H} (amide A)=3352–3471 (broad band), $\nu_{C=O}$ (amide I)=1609 cm⁻¹, and ν_{N-H} (amide II)=1558 cm⁻¹, respectively, upon changing the solvent from CHCl₃ to D₂O (Figure 5b). This shift in stretching and bending frequencies in D₂O indicates the involvement of intermolecular hydrogen bonding between the carbonyl (C=O) and amide N–H (i.e., C=O...N–H) during the self-assembled gelation. Now it is important to know whether inclusion of SWNTs/GO in the hydrogels

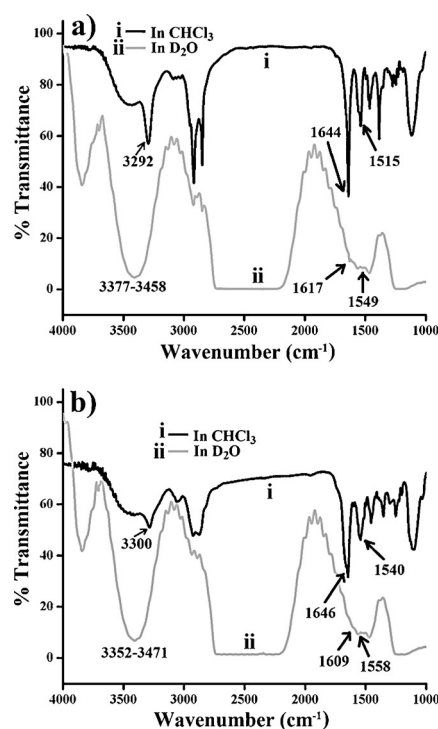


Figure 5. FTIR spectra of a) 1 and b) 4 in the respective solvents.

of amphiphiles 1 and 4 affected the self-assembly of the gelators. Interestingly, for the xerogel of the SWNT-incorporated hydrogel 1, the amide I and amide II peaks were found to be in a similar region, 1643 and 1520 cm⁻¹, respectively (Figure S4, Supporting Information) to that of the native gel in D₂O. In the case of the 4-GO composites, the peaks appeared at 1644 and 1542 cm⁻¹ (Figure S4, Supporting Information), whereas 4-SWNT showed analogous transmittance signals to its native hydrogel 4. Hence, it is evident that the integration of 1D and 2D carbon nanomaterials within the gel matrix did not perturb the intermolecular noncovalent interactions between gelators in the self-assembled state.^[11]

NMR spectroscopy

The ¹H NMR study provides information about the participation of various interacting forces such as intermolecular hydrogen bonding, hydrophobic interactions, and so on, between the self-aggregating molecules.^[10b,j] Accordingly, we performed temperature-dependent (Figure 6a and b) and solvent-dependent ¹H NMR experiments (Figure 6c and d) for gelators 1 and 4. The temperature-dependent ¹H NMR spectra of 1 (Figure 6a) in the gel state (in D₂O) at 25 °C showed that all the aromatic protons of the phenyl ring are broad in nature in the region $\delta=6.95$ –7.13 ppm. This broadening of the aromatic proton may have occurred because the hydrophobic interaction between the phenyl rings and the aromatic proton became more shielded. With increasing temperature, the interaction gradually decreased, and more sharp and downfield-shifted ($\delta=7.49$ –7.63 ppm at 85 °C) aromatic protons were observed. Similar observations were made in the case of 4 in D₂O (Figure 6b):

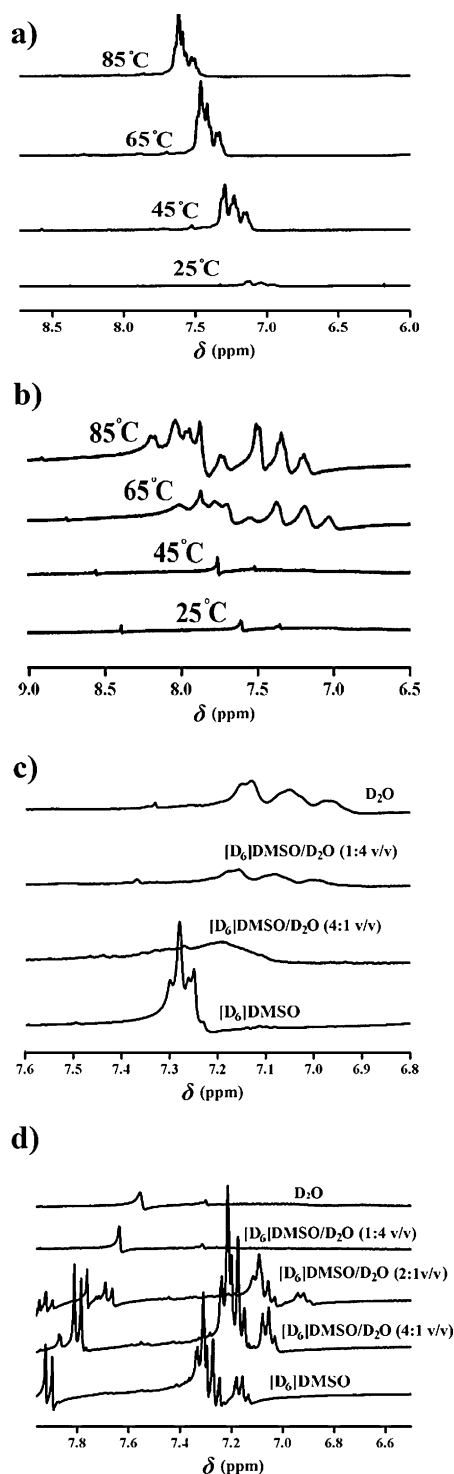


Figure 6. Temperature-dependent ^1H NMR spectra of a) **1** and b) **4**. Solvent-dependent ^1H NMR spectra of c) **1** and d) **4**.

a low-intensity broad peak was found for the aromatic region in the gel state at 25°C . The amide proton (N–H) of gelator **4** appeared at $\delta = 7.6$ ppm in the gel state, and the amide protons are very much shielded owing to its participation in intermolecular hydrogen bonding with the C=O group. The aromatic pyrenyl protons were also broadened owing to efficient π – π stacking interactions. With increasing temperature, the inter-

molecular hydrogen bond and the π – π stacking was ruptured. As a consequence, downfield shifts of aromatic and amide protons were observed at $\delta = 7.14$ – 7.98 ppm and $\delta = 8.12$ – 8.16 ppm, respectively, with increasing sharpness in the peak intensities. Interactions between aromatic rings during the gelation process were further investigated through solvent-dependent ^1H NMR experiments. In $[\text{D}_6]\text{DMSO}$, the aromatic proton of gelator **1** (molecularly dissolved state) showed a sharp peak in the region $\delta = 7.25$ – 7.30 ppm (Figure 6c). The D_2O content of the system was increased gradually from 20 to 100%. As a result, the NMR signals of the aromatic protons became broadened, along with a lowering of the δ value in the region 6.96– 7.14 ppm. Similar observations were found in the case of gelator **4** (Figure 6d), for which an upfield shift of aromatic protons was observed with widening of peaks upon increasing the D_2O content. In $[\text{D}_6]\text{DMSO}$, the lack of noncovalent interactions makes the gelator **1** molecules non-interactive with each other for self-assembly. With a gradual increase in D_2O content, initiation of self-aggregation occurred, facilitating the π – π interaction between the phenyl rings of the L-phenylalanine moiety. Similarly, in the case of gelator **4**, there was no π – π stacking with the pyrenyl moiety in $[\text{D}_6]\text{DMSO}$, and hence, a characteristic aromatic proton was observed in the region $\delta = 7.13$ – 7.33 . With a gradual increase in D_2O content, effective π – π stacking is initiated, resulting in the shielding of aromatic protons and a notable diminishing of the peak intensities.^[10b,j] The abovementioned spectroscopic and microscopic experiments delineate the participation of several noncovalent interactions in the self-assembled hydrogelation of **1** and **4**.

UV–visible spectroscopy

The aggregation pattern of small-molecule gelators was also investigated through a solvent-dependent UV/Vis spectroscopy study. The aggregation behavior of molecules is mainly categorized by two types: *H*-type and *J*-type.^[14] Molecules may self-assemble through parallel plane-to-plane stacking to form a sandwich-type array, which is referred to as *H*-type aggregation.^[14a] Alternatively, they may form a head-to-tail arrangement (end-to-end stacking), referred to as *J*-type aggregation. In UV/Vis spectra, *H*-aggregates with side-by-side alliance of molecules show a blueshifted absorption, whereas *J*-aggregates with the head-to-tail alignment exhibit a redshifted absorption from that of the monomer units.^[14] At this stage, we were keen to monitor the self-aggregation type of gelators **1** and **4**. As gelator **1** was devoid of any fluorescent moiety in its structure, we hydrophobically tagged one fluorescent probe, 8-anilino-1-naphthalenesulfonic acid (ANS), in **1** (ANS-**1**). The hydrophobic probe ANS is supposed to interact with the hydrophobic part of **1** and to localize itself at the hydrophobic domain of the aggregate.^[10j] Gelator **4** comprised an intrinsically UV-active pyrenyl moiety, so no external fluorophore was needed to follow its UV/Vis spectra. We recorded the UV/Vis spectra of ANS-**1** ($[\mathbf{1}] = 0.005 \text{ mg mL}^{-1}$, $[\text{ANS}] = 1 \times 10^{-6} \text{ M}$) and **4** (0.005 mg mL^{-1}) (Figure 7) in various solvents from non-gelating (DMSO) to a gelating one (water). ANS-**1** showed a broad band at 367 nm in DMSO, which was redshifted to 380 nm

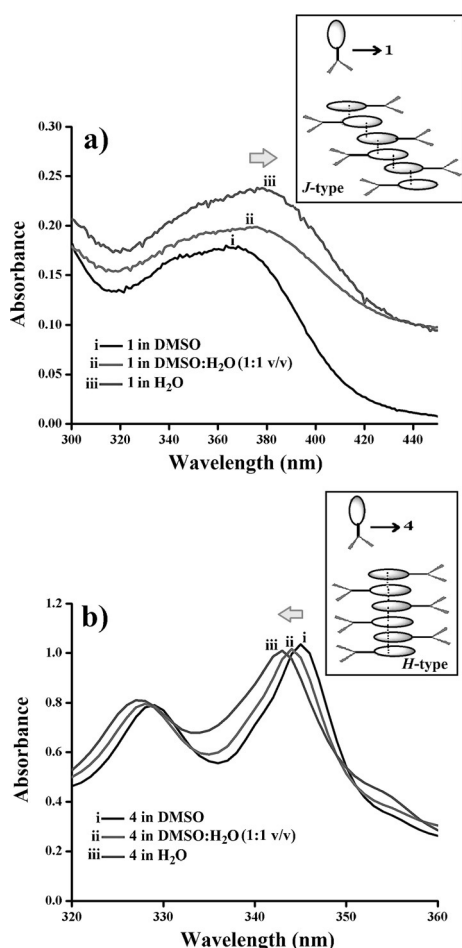


Figure 7. UV/Vis spectra of a) ANS-tagged gelator **1** and b) native gelator **4** in different solvents.

upon changing the solvent to milli-Q water (Figure 7a). This redshift clearly indicates the *J*-type aggregation pattern of **1** (Figure 8).^[14b,c] Presumably, this distinct *J*-type self-assembly of gelator **1** assisted spiral coiling in the gel fibers, as observed from the TEM image (Figure S2, Supporting Information). Interestingly, gelator **4** (0.005 mg mL⁻¹) in non-gelating solvent (DMSO) showed a sharp band of pyrene at 328 and 345 nm attributed to π - π^* transitions (Figure 7b). Upon changing the solvent system from DMSO to water, the π - π^* transition bands

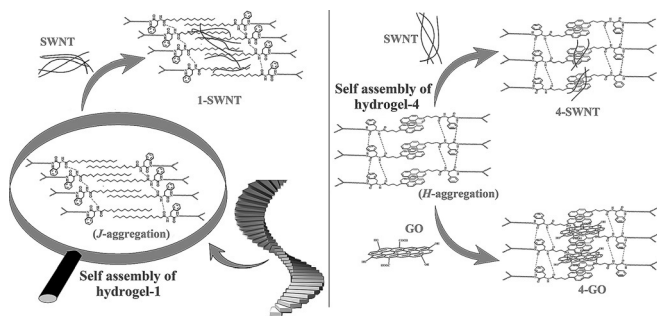


Figure 8. Pictorial representation of the self-assembly of hydrogels **1** and **4** and inclusion of SWNTs and GO.

were blueshifted to 325 and 340 nm, respectively. This suggests that the self-assembly occurred through *H*-type aggregation, that is, sandwich-type parallel layer formation (Figure 8).^[14a] This distinctive parallel layer-by-layer orientation of hydrogelator **4** probably aided successful GO inclusion in the hydrogel **4** matrix compared with that in other hydrogels. Consequently, it may be inferred that *J*-type aggregation helped to integrate only the 1D allotrope of carbon, and that *H*-type self-aggregation would be suited well for incorporation of both 1D and 2D allotropes of carbon (Figure 8).

Fluorescence study

Hydrophobic interaction is a much-discussed phenomenon in self-assembled hydrogelation. To this end, we performed a fluorescence spectroscopy study using 8-anilino-1-naphthalenesulfonic acid (ANS) during the hydrogelation of **1** (Figure 9a). ANS has an emission maximum (λ_{max}) at 509 nm in water upon excitation at 365 nm. The fluorescence intensity of ANS increased in the presence of **1**, and was enhanced gradually as the concentration of **1** was increased from 0.015 to 0.6 mg mL⁻¹. The increase in fluorescence intensity was accompanied by a blueshift from 509 to 479 nm (Figure 9a). Notably, the λ_{max} intensity decreased with a blueshift at 470 nm upon a further increase in the gelator concentration to 1.5 mg mL⁻¹. The above results indicate that upon self-assembly of **1**, ANS started to experience a hydrophobic environment. However, the fluorescent probe experienced a less hydrophobic environment in the gel state than in the intermediate state of gelation.^[10,15] Thus, the gelation process seemed to occur via an intermediate state of self-assembly to which ANS had a superior binding affinity compared with that in the gel state. In the case of gelator **4**, at a concentration of 0.01 mg mL⁻¹ (\approx 1000 times lower than MGC), a strong emission maximum was found at 397 nm, along with other peaks at 378 and 419 nm, upon excitation at 340 nm (Figure 9b). At this concentration, the molecule is evidently in a non-self-assembled state, in accordance with the characteristic emission spectrum of **4**. Upon increasing the gelator concentration to 0.1 mg mL⁻¹, a new excimer peak was formed at a higher wavelength ($\lambda = 469$ nm), possibly because of the π - π interactions between the pyrene moieties in the self-assembled state.^[10b,11b] Also, the bathochromic shift in fluorescence emission maximum is attributed to the strong intermolecular hydrogen bonding between the LMWG molecules. Furthermore, we recorded the fluorescence spectra of CNM-included hydrogel **4** (0.5 mg mL⁻¹), keeping the SWNT and GO concentrations fixed at 0.5 and 0.075 mg mL⁻¹, respectively (Figure 9c). Quenching of fluorescence intensity was evident from the emission spectra of both the SWNT- and GO-included gel nanohybrid compared with that of the native hydrogel. The reduced intensity in the fluorescence spectra of the **4**-SWNT and **4**-GO hybrids confirmed the successful integration of nanotubes and nanosheets within the SAFIN of the gel. The possible interaction between the hydrophobic pyrene moiety and aromatic backbone of SWNT/GO resulted in the quenching of fluorescence intensity.^[10b,11b] Moreover, the decrease in fluorescence emission intensity can also be observed visually. The

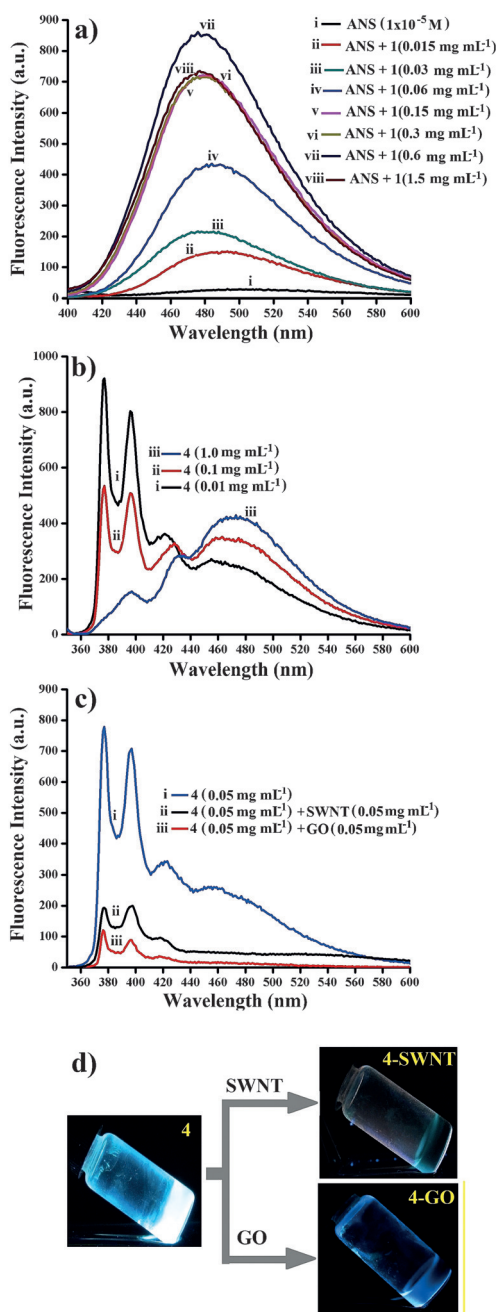


Figure 9. Fluorescence spectra of a) ANS ($[ANS] = 1 \times 10^{-5} \text{ M}$) tagged with **1**, and b) **4** with various concentrations. c) Fluorescence quenching of **4** upon inclusion of SWNTs and GO within the self-assembly. Photographic images of d) **4**, **4**-SWNT, and **4**-GO upon irradiation with a UV torch.

bright blue emission of the native hydrogel **4** upon UV irradiation (365 nm) was reduced significantly upon inclusion of SWNTs/GO in the gel matrix (Figure 9d).

Steady-state fluorescence anisotropy

Steady-state fluorescence anisotropy is an excellent tool for measuring the fluidity of a system using a fluorescence probe. The most common probe used to measure fluorescence anisotropy is 1,6-diphenyl-1,3,5-hexatriene (DPH), which intercalates

between the hydrophobic interior of the aggregates thanks to its rod-like shape and hydrophobic nature.^[16a] The higher steady-state anisotropy (r) value indicates the restricted movement of DPH in various aggregated structures.^[16b,c] We used this technique to understand the gelation mechanism of **1**. It is observed that at a low concentration of **1** (0.20 mg mL^{-1}) in water, DPH showed a relatively large r value (0.13, Table 3). At

Table 3. Steady-state fluorescence anisotropic (r) values of DPH for gelator **1** in water.

Concentration of gelator 1 [mg mL^{-1}]	r
0.20	0.13
0.30	0.10
0.60	0.10
1.50	0.10
3.00	0.10

a lower concentration of the amphiphile (below or around the critical micellar concentration, cmc), DPH molecules aggregate with each other, showing a higher anisotropy.^[10,16d] However, the r value remained unaltered ($r=0.10$, Table 3) with increasing concentrations of **1** ($0.30\text{--}3.0 \text{ mg mL}^{-1}$, Table 3). Presumably, above the cmc, DPH molecules become solubilized in the hydrophobic interior of the micelles with lower microviscosity.^[10] Notably, in the case of a micellar solution of common surfactant, cetyltrimethylammonium chloride (CTAC), within the concentration range $5\text{--}100 \text{ mM}$, the r value was found to be 0.06. The higher anisotropy for **1** ($r=0.10$) compared with that for CTAC ($r=0.06$) indicates that the aqueous solution of **1** is a more viscoelastic system. The microviscosity of the solution of **1** is higher, probably because of the formation of elongated micelles (rod- or worm-like).^[10] On the basis of the above observation, it may be inferred that the formation of the hydrogel of **1** ($\text{MGC} = 15 \text{ mg mL}^{-1}$) is processed by changing the topology from elongated micelles to a fibrillar network upon increasing the concentration of **1**. We were unable to perform the fluorescence anisotropy experiment with gelator **4** because it contains the intrinsically fluorescent pyrene unit, which interferes in the anisotropy experiment as the excitation wavelength of pyrene is comparable with that of DPH ($\lambda_{\text{ex}} = 370 \text{ nm}$).

Rheology

At this point, it would be fascinating to determine how the stiffness of the gel changed upon addition of CNM to the gel matrix. Rheological studies provide information on the fluidity and rigidity of viscoelastic materials such as gels.^[10a] Two major parameters related to viscoelasticity are the storage modulus (G') and the loss modulus (G''). The storage modulus G' indicates the ability of a deformed material to restore its native form, whereas the loss modulus G'' represents the flow behavior of the material under applied stress.^[10a,b] For viscoelastic materials such as gels, $G' > G''$ (G' and $G'' = \omega^0$, $\omega = \text{angular frequency}$), and in the sol state, $G'' > G'$ ($G' = \omega^2$ and $G'' = \omega$). Ini-

tially, we studied the mechanical stiffness of native hydrogels **1** and **4** at their respective MGCs (15 and 10 mg mL⁻¹, respectively) through an oscillatory frequency-sweep experiment, in which G' and G'' were recorded as a function of angular frequency (in the range 0.1–600 rad s⁻¹) at a fixed strain of 0.01 % (Figure 10). Native hydrogels **1** and **4** exhibited G' values of 410 and 585 Pa, respectively. Interestingly, upon inclusion of pristine SWNTs into hydrogel **1**, the value of G' increased two-fold ($G' = 805$ Pa) compared with the native gel at SWNT concentration of 1.5 mg mL⁻¹. On the other hand, the GO-included (1.5 mg mL⁻¹) hydrogel **4** showed a mere 1.06-fold improvement in G' value ($G' = 622$ Pa). However, **4**-GO with 3 mg mL⁻¹ GO content showed approximately 1.7-fold ($G' = 988$ Pa) enhanced mechanical rigidity compared with that of the native hydrogel. The above results indicate that the enhanced cross-linking between SWNTs/GO and the SAFIN led to better mechanical resistance of the soft nanocomposites.

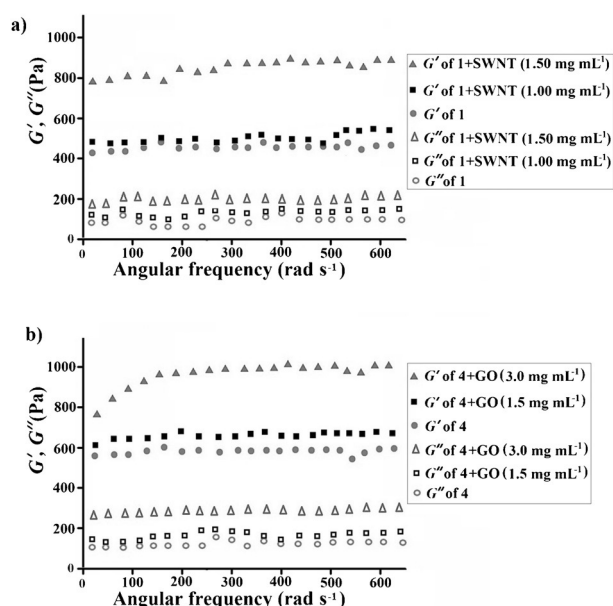


Figure 10. Plots of G' and G'' of a) hydrogel-1 and 1-SWNT and b) hydrogel-4 and 4-GO.

Conclusions

In brief, TEG-attached neutral hydrogelators containing L-phenylalanine tailored with suitable hydrophobic residues were synthesized. These gelators self-assembled to form hydrogels in water and aqueous buffer solutions (pH 3–7). The critical role of HLB in self-assembled gelation was analyzed by altering the hydrophobic residue from a long chain (C-16) to an extended aromatic pyrenyl group. Moreover, the involvement of various interactions in the gelation and the structure-dependent inclusion of 1D and 2D allotropes of carbon nanomaterials within the SAFIN was investigated through spectroscopic and microscopic studies. Interestingly, the C-16-containing gelator **1** can successfully include the 1D allotrope of carbon (SWNTs), whereas the pyrene-containing gelator **4** includes both 1D and 2D allotropes of carbon (SWNTs and GO, respec-

tively). The J -type and H -type self-aggregation patterns of hydrogelators **1** and **4**, respectively, might have facilitated the structure-dependent inclusion of CNMs within the hydrogel. Hence, the modulation of the hydrophobic terminus of the gelator has a notable influence on its self-aggregation as well as its integration of CNMs of different dimensions. Moreover, rheological studies of the hydrogels and SWNT/GO-gel composites show that the inclusion of SWNTs/GO within the hydrogel improves the mechanical stiffness of the resulting soft nanocomposites compared with that of the native hydrogel.

Experimental Section

Materials

L-Phenylalanine, naphthalene-1-acetic acid, dicyclohexylcarbodiimide (DCC), 4-*N,N*-(dimethyl)aminopyridine (DMAP), 1-hydroxybenzotriazole (HOBT), di-*tert*-butyldicarbonate (BOC anhydride), silica gel 60–120 and 100–200 mesh, and solvents were purchased from SRL, India. Trifluoroacetic acid (TFA) and sodium hydroxide pellets, potassium carbonate, and thionyl chloride were bought from Spectrochem, India. Palmitic acid, 1-pyrenebutyric acid, 2,2'-(ethylene-dioxy) bis(ethylamine), triethylene glycol monomethyl ether (TEG), tosyl chloride, single-walled carbon nanotubes (SWNTs), graphite powder, CDCl₃, [D₆]DMSO, and D₂O were procured from Sigma. All deuterated solvents for NMR and FTIR experiments were obtained from Aldrich Chemical Co. Thin-layer chromatography was performed on Merck pre-coated silica gel 60-F₂₅₄ plates. Lyophilization was performed in a Virtis 4 KBTXL-75 freeze-drier. Mass spectrometric data were acquired through the electron spray ionization (ESI) technique on a Q-tof-micro quadrupole mass spectrometer (Micromass). ¹H NMR spectra were recorded with an AVANCE 500 MHz (Bruker) spectrometer. Elemental analyses were performed with a PerkinElmer 2400 CHN analyzer. High-resolution transmission electron microscopy (TEM) images were taken on a JEOL JEM2010 high-resolution microscope operating at 200 kV. Field-emission scanning electron microscopy (SEM) was performed with a JEOL-6700F microscope. The UV/Vis absorption spectra were recorded on a PerkinElmer Lambda 25 spectrophotometer. Fluorescence spectra were recorded with a Varian Cary Eclipse luminescence spectrometer, and FTIR spectra were recorded on a Perkin-Elmer Spectrum 100 spectrometer. XRD measurements were made with a Seifert XRD 3000P diffractometer, with CuK_α radiation ($\alpha = 0.15406$ nm) with a voltage and current of 40 kV and 30 mA, respectively. Probe sonication and bath sonication were performed with an Omni Sonic Ruptor 250 and Telsonic Ultrasonic bath sonicator, respectively.

Synthesis of amphiphilic gelators 1–4

All the amphiphiles were synthesized by following well established peptide chemistry (Schemes S1 and S2, Supporting Information). The carboxylic acid group of the L-phenylalanine was converted to a methyl ester. The ester-protected amino acid was coupled with palmitic acid with DCC (1 equiv), DMAP (cat.), and HOBT (1 equiv) in dry DCM (CH₂Cl₂). The ester-protected amide was purified by column chromatography on 60–120 mesh silica gel (methanol/chloroform). The product was then hydrolyzed by treating with 1N NaOH solution (1.1 equiv) in MeOH for 6 h with stirring at room temperature. The reaction mixture was concentrated on a rotary evaporator, and then diluted with water. The aqueous mixture was washed with diethyl ether and subsequently acidified with a 1N

aqueous HCl solution, and the produced carboxylic acid was extracted with ethyl acetate. This acid was coupled with mono-Boc-protected 2,2'-(ethylenedioxy)bis(ethylamine) by treating it with DCC (1 equiv), DMAP (cat.), and HOBt (1 equiv) in dry CH_2Cl_2 . The product was purified by column chromatography on 100–200 mesh silica gel (methanol/chloroform). The purified product was subjected to deprotection of Boc for 3 h by stirring with trifluoroacetic acid (TFA; 4 equiv) in dry DCM. The solvent was removed on a rotary evaporator and the mixture was taken in ethyl acetate (EtOAc). The EtOAc part was washed thoroughly with 10% aqueous sodium carbonate (Na_2CO_3) solution followed by brine to neutrality. The organic part was dried over anhydrous sodium sulfate and concentrated to obtain the corresponding amine. The product was purified by column chromatography on 100–200 mesh silica gel (methanol/chloroform as eluent). In the final step, the pure amine was subjected to nucleophilic substitution under reflux conditions in dry acetonitrile (CH_3CN) in the presence of anhydrous K_2CO_3 (2.5 equiv) at 70 °C, to obtain the hydrophilic triethylene glycol monomethyl ether (TEG)-substituted product. Accordingly, the reaction mixture was filtered, and the desired product (**1**) was purified by column chromatography on 100–200 mesh silica gel (methanol/chloroform). A similar protocol was applied to synthesize **2–4** using C-16-chain-protected L-phenylalanine, naphthalene-1-acetic acid, and 1-pyrenebutyric acid (Schemes S1 and S2, Supporting Information). ^1H NMR spectroscopic and mass spectroscopic analysis of **1**, **2**, **3**, and **4** are provided in the Supporting Information.

Preparation of hydrogels

The requisite amounts of **1**, **3**, and **4** were taken in screw-capped vials (internal diameter, i.d., of 10 mm) and heated slowly to dissolve in Milli-Q water and in various phosphate-HCl buffer solutions (pH 3.0–7.0). The gelation ability of **2** was tested in DMSO- H_2O (1:3, v/v). The solution was allowed to cool slowly (undisturbed) to room temperature. The gelation was checked through the “stable-to-inversion” test of the aggregated materials in the glass vials.

Determination of gel-to-sol transition temperature (T_{gel})

The gel-to-sol transition temperature (T_{gel}) was recorded by gradually increasing the temperature (at a rate of 2 °C min^{-1}) in a thermostatted oil bath in which the hydrogel-containing glass vial (i.d. 10 mm) was placed. The temperature (± 0.5 °C) at which the gel liquified and started to flow under gravitation is referred to as T_{gel} .

Synthesis of graphene oxide (GO)

Graphene oxide (GO) was synthesized from graphite powder (<30 mm) following the modified Hummer's method. Graphite powder (0.5 g) was dispersed in concentrated H_2SO_4 (20 mL), sodium nitrate (0.5 g) was added to the dispersion, and this was then cooled to 0 °C. Subsequently, KMnO_4 (1.5 g) was added slowly to the mixture so that the temperature remained below 20 °C, and mixed thoroughly. The resulting solution was transferred to a water bath at 35 °C and stirred for 30 min. The temperature was raised to 90 °C during the addition of water (30 mL), and was maintained for a further 15 min. The whole solution was then mixed in warm water (80 mL). To this solution, 30% H_2O_2 (0.5 mL) was added to reduce the residual permanganate. The solution was filtered and washed thoroughly with warm water. The solid was dispersed in distilled water (100 mL) by sonication. This dispersion was centrifuged at 3000 rpm for 15 min. The residue was suspended

in water by sonication and again centrifuged at 20000 rpm. This suspension/centrifugation process was repeated twice. Finally the semi-solid residue was collected and freeze-dried in vacuum to obtain GO. The formation of GO was further characterized by UV/Vis spectroscopy and X-ray diffraction (XRD).

Preparation of SWNT/GO-included gel nanocomposites

The required amount of SWNTs was weighed in a screw-capped glass vial (i.d. 10 mm). An aqueous solution (1 mL) of amphiphile (**1** and **4**) of the required concentration was added, and the mixture was tip-sonicated for 10 min at 30% power output. The solution was then left undisturbed for 30 min to form a nanohybrid gel (1-SWNT and 4-SWNT) that was stable to the inversion of the glass vial. A similar protocol was followed for the preparation of the GO-included nanocomposite (4-GO). The required amount of GO was weighed and an aqueous solution of amphiphile **4** (1 mL) of the desired concentration was added and again tip-sonicated for 10 min at 40% power output. The solution was kept carefully at room temperature for half an hour to prepare the soft nanocomposite (4-GO) having restricted mobility of the solvent.

Microscopic study

Field-emission SEM images were obtained on a JEOL-6700F microscope. A drop of gel (at the MGC) was placed on a piece of cover slip and dried for a few hours under vacuum before imaging. TEM experiments were performed on a JEOL JEM2010 high-resolution microscope operated at an accelerating voltage of 200 kV. A dilute solution of gel was placed on a 300 mesh carbon-coated Cu grid and dried for a few hours under vacuum before imaging.

Circular dichroism

CD spectra of aqueous solutions of gelators **1**, **3**, and **4** at varying concentrations were recorded by using a quartz cuvette of 1 mm path length in a JASCO J-815 CD spectropolarimeter.

FTIR measurements

FTIR measurements were performed with gelators in the non-self-assembled state in CHCl_3 , in the gel state in D_2O , and in dried condition for hydrogels **1** and **4** as well as for SWNT/GO nanocomposites (1-SWNT, 4-SWNT, and 4-GO) at room temperature. All the experiments were performed with a PerkinElmer Spectrum 100 FTIR spectrometer using KBr pellets (for CHCl_3 solutions and xerogels) or a 1 mm CaF_2 cell (for D_2O gels).

Temperature- and solvent-dependent ^1H NMR measurements

Temperature-dependent ^1H NMR spectra of **1** and **4** were recorded on an Avance 300 MHz (Bruker) spectrometer at a concentration of 15 and 10 mg mL^{-1} , respectively, in D_2O at various temperatures (25–85 °C). Solvent-dependent ^1H NMR spectra of **1** and **4** were also recorded at the MGC for both **1** and **4** in various solvent ratios of D_2O and $[\text{D}_6]\text{DMSO}$.

UV/Vis spectroscopy

The UV/Vis spectra of ANS-doped gelator **1** and native gelator **4** were recorded on a PerkinElmer Lambda 25 spectrophotometer by varying the solvent from a non-gelating (DMSO) to a gelating one (Milli-Q water).

Fluorescence spectroscopy

The emission spectra of ANS and aqueous solutions of ANS-doped hydrogel **1** were recorded with a Varian Cary Eclipse luminescence spectrometer. The probe molecules were added to the aqueous solutions of amphiphiles at various concentrations at room temperature. ANS stock solution was prepared in MeOH; from this super stock solution, the required amount of ANS solution was added to the gelators so that the final concentration of ANS solution was 1×10^{-5} M. The ANS solution was excited at 360 nm (λ_{ex}). A fluorescence study of gelator **4** was performed by recording the spectra of the amphiphilic solution excited at 340 nm (λ_{ex}) at various gelator concentrations. The excitation and emission slit widths were both 5 nm.

Steady-state fluorescence anisotropy study

The steady-state fluorescence anisotropy study was performed using the fluorescent probe DPH in an aqueous solution of surfactant with a Varian Cary Eclipse luminescence spectrometer. A stock solution of DPH was prepared in tetrahydrofuran (THF), keeping the final DPH concentration at 2×10^{-6} M. The aqueous solutions were excited at 370 nm for DPH, and the corresponding emission spectra were recorded at 450 nm. The excitation and emission slit widths were 2.5 and 5 nm, respectively. The fluorescence anisotropic value (r) was calculated by the instrumental software using Equation (1), in which I_{VV} and I_{VH} are, respectively, the fluorescence intensities of the emitted light polarized parallel and perpendicular to the excited light, and $G = I_{\text{VV}}/I_{\text{VH}}$ is the instrumental grating factor.

$$r = (I_{\text{VV}} - GI_{\text{VH}})/(I_{\text{VV}} + 2GI_{\text{VH}}) \quad (1)$$

The fluorescence measurements were performed at 25 °C.

Rheology

Rheological experiments were performed in cone and plate geometry (diameter 40 mm) on the rheometer plate using an Anton Paar MCR302 instrument. The native gels (**1** and **4**) and the SWNT-gel (**1**-SWNT) and GO-gel (**4**-GO) composites were scooped on the rheometer plate so that there was no air gap with the cone. Frequency sweep experiments were performed as a function of angular frequency (0.1–200 rads^{-1}) at a fixed strain of 0.01% at 25 °C, and the storage modulus (G') and loss modulus (G'') were plotted against angular frequency (ω).

Acknowledgements

PKD thanks the Department of Science and Technology, India (SR/S1/OC-25/2011) for financial assistance. PC, DM, and SB acknowledge the Council of Scientific and Industrial Research, India for Research Fellowships.

Keywords: amphiphiles • carbon nanomaterials • hydrogels • neutral gelators • self-assembly • soft nanocomposites

- [1] a) D. Ma, K. Tu, L. M. Zhang, *Biomacromolecules* **2010**, *11*, 2204; b) D. M. Ryan, B. L. Nilsson, *Polym. Chem.* **2012**, *3*, 18.
[2] a) M. J. Wilson, S. J. Liliensiek, C. J. Murphy, W. L. Murphy, P. F. Nealey, *Soft Matter* **2012**, *8*, 390; b) D. Kalafatovic, M. Nobis, N. Javid, P. W. J. M.

- Frederix, K. I. Anderson, B. R. Saunders, R. V. Ulijn, *Biomater. Sci.* **2015**, *3*, 246.
[3] a) E. Caló, V. V. Khutoryanskiy, *Eur. Polym. J.* **2015**, *65*, 252; b) J. Wang, *Anal. Chim. Acta* **1999**, *399*, 21.
[4] a) C. C. Beozzo, M. A. Alves-Rosa, S. H. Pulcinelli, C. V. Santilli, *Materials* **2013**, *6*, 1967; b) R. Kumar, K. Jayaramulu, T. K. Maji, C. N. R. Rao, *Dalton Trans.* **2014**, *43*, 7383; c) A. Chakrabarty, U. Maitra, *J. Phys. Chem. B* **2013**, *117*, 8039; d) P. K. Vemula, G. John, *Chem. Commun.* **2006**, 2218.
[5] a) S. K. Samanta, S. Bhattacharya, *J. Mater. Chem.* **2012**, *22*, 25277; b) Y. M. Abul-Haija, R. V. Ulijn, *Biomacromolecules* **2015**, *16*, 3473; c) J. M. Poolman, J. Boekhoven, A. Besselink, A. G. L. Olive, J. H. van Esch, R. Eelkema, *Nat. Protoc.* **2014**, *9*, 977; d) B. Escuder, F. Rodríguez-Llansola, J. F. Miravet, *New J. Chem.* **2010**, *34*, 1044; e) J. D. Decoppet, T. Moehl, S. S. Babkair, R. A. Alzubaydi, A. A. Ansari, S. S. Habib, S. M. Zakeeruddin, H. W. Schmidt, M. Grätzel, *J. Mater. Chem. A* **2014**, *2*, 15972.
[6] a) D. Das, T. Kar, P. K. Das, *Soft Matter* **2012**, *8*, 2348; b) S. Srinivasan, V. K. Praveen, R. Philip, A. Ajayaghosh, *Angew. Chem. Int. Ed.* **2008**, *47*, 5675; *Angew. Chem.* **2008**, *120*, 5759; c) A. T. Haedler, K. Kreger, A. Issac, B. Wittmann, M. Kivala, N. Hammer, J. Köhler, H. W. Schmidt, R. Hildner, *Nature* **2015**, *523*, 196; d) I. Sittko, K. Kremser, M. Roth, S. Kuehne, S. Stuhr, J. C. Tiller, *Polymer* **2015**, *64*, 122; e) S. Bhattacharjee, S. K. Samanta, P. Moitra, K. Pramoda, R. Kumar, S. Bhattacharya, C. N. R. Rao, *Chem. Eur. J.* **2015**, *21*, 5467; f) C. Krumm, S. Harmuth, M. Hijazi, B. Neugebauer, A. L. Kampmann, H. Geltenpoth, A. Sickmann, J. C. Tiller, *Angew. Chem. Int. Ed.* **2014**, *53*, 3830; *Angew. Chem.* **2014**, *126*, 3908; g) J. Gao, H. Wang, L. Wang, J. Wang, D. Kong, Z. Yang, *J. Am. Chem. Soc.* **2009**, *131*, 11286.
[7] a) D. Mandal, S. K. Mandal, P. K. Das, *Chem. Eur. J.* **2015**, *21*, 12042; b) B. Xing, C. W. Yu, K. H. Chow, P. L. Ho, D. Fu, B. Xu, *J. Am. Chem. Soc.* **2002**, *124*, 14846; c) H. Kobayashi, A. Friggeri, K. Koumoto, M. Amai, S. Shin-kai, D. N. Reinhoudt, *Org. Lett.* **2002**, *4*, 1423; d) L. A. Estroff, A. D. Hamilton, *Angew. Chem. Int. Ed.* **2000**, *39*, 3447; *Angew. Chem.* **2000**, *112*, 3589.
[8] a) A. S. Hoffman, *Adv. Drug Delivery Rev.* **2012**, *64*, 18; b) J. Bergera, M. Reista, J. M. Mayera, O. Felb, N. A. Peppas, R. Gurny, *Eur. J. Pharm. Biopharm.* **2004**, *57*, 19; c) S. Brahmachari, D. Das, P. K. Das, *Chem. Commun.* **2010**, *46*, 8386; d) F. Zhao, M. L. Ma, B. Xu, *Chem. Soc. Rev.* **2009**, *38*, 883; e) G. Liang, Z. Yang, R. Zhang, L. Li, Y. Fan, Y. Kuang, Y. Gao, T. Wang, W. W. Lu, B. Xu, *Langmuir* **2009**, *25*, 8419; f) Y. Tian, H. Wang, Y. Liu, L. Mao, W. Chen, Z. Zhu, W. Liu, W. Zheng, Y. Zhao, D. Kong, Z. Yang, W. Zhang, Y. Shao, X. Jiang, *Nano Lett.* **2014**, *14*, 1439.
[9] a) S. S. Babu, V. K. Praveen, A. Ajayaghosh, *Chem. Rev.* **2014**, *114*, 1973; b) K. Naoi, S. Ishimoto, J. Miyamoto, W. Naoi, *Energy Environ. Sci.* **2012**, *5*, 9363; c) G. Vilaça, B. Jousseau, C. Mahieux, C. Belin, H. Cachet, M. C. Bernard, V. Vivier, T. Toupance, *Adv. Mater.* **2006**, *18*, 1073; d) H. Li, J. Choi, T. Nakanishi, *Langmuir* **2013**, *29*, 5394; e) D. Depan, A. P. Kumar, R. P. Singh, *Acta Biomater.* **2009**, *5*, 93.
[10] a) T. Kar, S. K. Mandal, P. K. Das, *Chem. Commun.* **2012**, *48*, 8389; b) D. Mandal, T. Kar, P. K. Das, *Chem. Eur. J.* **2014**, *20*, 1349; c) R. Liu, S. M. Mahurin, C. Li, R. R. Unocic, J. C. Idrobo, H. Gao, S. J. Pennycook, S. Dai, *Angew. Chem. Int. Ed.* **2011**, *50*, 6799; *Angew. Chem.* **2011**, *123*, 6931; d) M. Tunckol, J. Durand, P. Serp, *Carbon* **2012**, *50*, 4303; e) X. Yang, G. Zhang, D. Zhang, J. Xiang, G. Yang, D. Zhu, *Soft Matter* **2011**, *7*, 3592; f) J. Liu, G. Chen, M. Jiang, *Macromolecules* **2011**, *44*, 7682; g) M. J. Allen, V. C. Tung, R. B. Kaner, *Chem. Rev.* **2010**, *110*, 132; h) J. I. Paredes, S. Villar-Rodil, A. Martínez-Alonso, J. M. D. Tascón, *Langmuir* **2008**, *24*, 10560; i) O. C. Compton, S. T. Nguyen, *Small* **2010**, *6*, 711; j) S. Dutta, A. Shome, S. Debnath, P. K. Das, *Soft Matter* **2009**, *5*, 1607.
[11] a) C. Maity, W. E. Hendriksen, J. H. van Esch, R. Eelkema, *Angew. Chem. Int. Ed.* **2015**, *54*, 998; *Angew. Chem.* **2015**, *127*, 1012; b) S. K. Mandal, D. Mandal, P. K. Das, *ChemPlusChem* **2015**, DOI: 10.1002/cplu.201500457; c) S. K. Samanta, K. S. Subrahmanyam, S. Bhattacharya, C. N. R. Rao, *Chem. Eur. J.* **2012**, *18*, 2890; d) J. Wu, A. Chen, M. Qin, R. Huang, G. Zhang, B. Xue, J. Wei, Y. Li, Y. Cao, W. Wang, *Nanoscale* **2015**, *7*, 1655.
[12] a) W. S. Hummers, R. E. Offeman, *J. Am. Chem. Soc.* **1958**, *80*, 1339; b) M. Yoshida, N. Koumura, Y. Misawa, N. Tamaoki, H. Matsumoto, H. Kawanami, S. Kazaoui, N. Minami, *J. Am. Chem. Soc.* **2007**, *129*, 11039.
[13] a) B. Escuder, J. F. Miravet, *Langmuir* **2006**, *22*, 7793; b) I. Laczko, E. Vass, K. Soós, L. Fülöp, M. Zarándi, B. Penke, *J. Pept. Sci.* **2008**, *14*, 731; c) N. J. Greenfield, *Nat. Protoc.* **2007**, *1*, 2876; d) C. A. Bush, S. K. Sarkar, K. D. Kopple, *Biochemistry* **1978**, *17*, 4951.

- [14] a) Y. Dong, B. Xu, J. Zhang, X. Tan, L. Wang, J. Chen, H. Lv, S. Wen, B. Li, L. Ye, B. Zou, W. Tian, *Angew. Chem. Int. Ed.* **2012**, *51*, 10782; *Angew. Chem.* **2012**, *124*, 10940; b) Y. Hirano, Y. Tokuoka, N. Kawashima, Y. Ozaki, *Vib. Spectrosc.* **2007**, *43*, 86; c) A. D'Urso, M. E. Fragala, R. Purrello, *Chem. Commun.* **2012**, *48*, 8165.
- [15] U. Maitra, S. Mukhopadhyay, A. Sarkar, P. Rao, S. S. Indi, *Angew. Chem. Int. Ed.* **2001**, *40*, 2281; *Angew. Chem.* **2001**, *113*, 2341.
- [16] a) A. J. C. Fulford, W. E. Peel, *Biochim. Biophys. Acta* **1980**, *598*, 237; b) S. Bhattacharya, Y. K. Ghosh, *Langmuir* **2001**, *17*, 2067; c) S. Mukhopadhyay, I. G. Krishnamoorthy, U. Maitra, *J. Phys. Chem. B* **2003**, *107*, 2189.

Received: December 4, 2015

Published online on February 24, 2016
